Galaxy Zoo DESI: large-scale bars as a secular mechanism for triggering AGN

Izzy L. Garland,[1]* Mike Walmsley,[2] Maddie S. Silcock,[1,3] Leah M. Potts,[1] Josh Smith,[1]
Brooke D. Simmons,[1] Chris J. Lintott,[4] Rebecca J. Smethurst,[4] James Dawson, Melanie Galloway,[5]
Karen L. Masters,[6] David O'Ryan,[1] Jürgen Popp,[7] Matthew R. Thorne,[1] GZ Team[8]

[1]*Physics Department, Lancaster University, Lancaster LA1 4YB, UK*
[2]*Jodrell Bank Centre for Astrophysics, Department of Physics & Astronomy, University of Manchester, Oxford Road, Manchester M13 9PL, UK*
[3]*Centre for Astrophysics Research, University of Hertfordshire, College Lane, Hatfield AL10 9AB, UK*
[4]*Oxford Astrophysics, Department of Physics, University of Oxford, Denys Wilkinson Building, Keble Road, Oxford OX1 3RH, UK*
[5]*Mel's House*
[6]*Departments of Physics and Astronomy, Haverford College, Lancaster Avenue, Ardmore, PA 19041 USA*
[7]*School of Physical Sciences, The Open University, Milton Keynes, MK7 6AA, UK*
[8] *Some Places*

ABSTRACT

Despite the evidence that supermassive black holes (SMBHs) co-evolve with their host galaxy, and that most of the growth of these SMBHs occurs via merger-free processes, the underlying mechanisms which drive this secular co-evolution are poorly understood. We investigate the role that both strong and weak large-scale galactic bars play in mediating this relationship. Using Galaxy Zoo DESI, we analyse the active galactic nucleus (AGN) fraction in strongly barred, weakly barred, and unbarred galaxies up to $z \leq 0.1$ over a range of stellar masses and colours. After controlling for stellar mass and colour, we find that the optically selected AGN fraction is 26.5 ± 0.8 percent in strongly barred galaxies, 17.8 ± 0.7 per cent in weakly barred galaxies, and 12.4 ± 0.6 per cent in unbarred disk galaxies. Strongly barred galaxies have a higher fraction of AGNs than weakly barred galaxies, which in turn have a higher fraction than unbarred galaxies. Thus, while bars are not required in order to grow a SMBH in a disc galaxy, large-scale galactic bars appear to facilitate AGN fuelling, and the presence of a strong bar makes a disc galaxy more than twice as likely to host an AGN at all galaxy stellar masses and colours.

Key words: galaxies: active – galaxies: bar – galaxies: disc – galaxies: Seyfert

1 INTRODUCTION

Supermassive black holes (SMBHs) reside in the centre of the majority of galaxies, gaining most of their mass during active phases, where the accretion systems are known as active galactic nuclei (AGNs). Yet what triggers the "switch on" of an AGN is unknown. This question is critical to understanding the interplay between AGNs and their host galaxies, including the effectiveness of AGN feedback and SMBH-galaxy co-evolution (see e.g., Kormendy & Ho 2013; Heckman & Best 2014, for a review).

Recent simulation studies have shown that the majority of SMBH growth occurs via secular (merger-free) mechanisms (Martin et al. 2018; McAlpine et al. 2020; Smethurst et al. 2023), meaning that mergers are not the primary drivers of the relationships known to exist between SMBHs and their host galaxies. Disc-dominated galaxies have had a history free from major mergers since at least $z \sim 2$ (Martig et al. 2012), and so by exclusively looking at a population of disc-dominated galaxies and the kiloparsec scale structures within them

(such as large-scale galactic bars), we can gain a better understanding of AGN triggering in the absence of major-mergers.

Large-scale strong bars are observed at optical wavelengths in the Sloan Digital Sky Survey (SDSS; York et al. 2000) in 29.4 ± 0.5 per cent of disc galaxies at redshift $0.01 < z < 0.06$ (Masters et al. 2011), and when using either a deeper optical survey or one with better seeing, such as DECaLS, this increases to around 45 per cent when combining galaxies with either weak or strong bars (Géron et al. 2021). This distinction between strong and weak bars is important, despite their being on a continuum, since work, e.g. by Géron et al. (2023), has shown that they may have different formation mechanisms. These bars can cause transfers of a disc's angular momentum, leading to gas being transported down to the inner central kiloparsec region (Friedli & Benz 1993; Athanassoula 2003), where it could be accreted onto a black hole. Thus, by tracing these kiloparsec-scale structures, we can gain insight into the dynamics within a galaxy that facilitate the transfer of angular momentum, and hence the fuelling which gives rise to the AGN characteristics that we observe.

Simulations have shown that it is physically possible for bars to provide the necessary inflow of gas to match the accretion rates we see in AGNs (Sakamoto 1996; Maciejewski et al. 2002; Regan &

* E-mail: i.garland@lancaster.ac.uk

Teuben 2004; Lin et al. 2013), and this is mirrored in observational work by Smethurst et al. (2021). Several other studies have pointed to either an increase in the bar fraction of AGN hosts compared to inactive galaxies, or an increase in AGN fraction in barred galaxies compared to unbarred (Knapen et al. 2000; Laine et al. 2002; Coelho & Gadotti 2011; Oh et al. 2012; Alonso et al. 2018; Galloway et al. 2015; Silva-Lima et al. 2022; Garland et al. 2023).

Many of these previous studies have suffered from low statistical significance or sensitivity to methodology and selection effects. There are also a number of studies finding no correlation (e.g. Cheung et al. 2013; Goulding et al. 2017). Thus, in this work, we aim to revisit this correlation between large-scale bars and AGNs, using Galaxy Zoo DESI (Walmsley et al., in press) to obtain robust morphologies from deeper imaging, and observed emission lines from SDSS MPA-JHU DR7[1] to determine the activity category of the systems in our sample.

Section 2 discusses our sample selection and classification. We present our results in Section 3, followed by our discussions and conclusions in Sections 4 and 5. Throughout this paper, the term "active galaxy" refers to a Seyfert galaxy, and the term "inactive galaxy" refers to a star-forming galaxy that does not host an AGN. We use WMAP9 cosmology (Hinshaw et al. 2013), where we assume a flat universe, $H_0 = 69.3 \, \mathrm{km \, s^{-1} \, Mpc^{-1}}$ and $\Omega_m = 0.287$.

2 DATA COLLATION

2.1 Sample Selection

Galaxy Zoo DESI (GZD; Walmsley et al. 2023b, accepted) uses machine learning to identify the morphology of the 8.7M galaxies in the DESI Legacy Imaging Surveys: DECaLS, MzLS and BASS, plus DES. Full details of the methodology can be found in the release paper, but we summarise briefly here.

Given the size of the DESI Legacy Imaging Surveys, it was not feasible to collect morphological classifications from volunteers alone (such as in Galaxy Zoo 2), as this would take around 200 years at current classification rates. Thus more efficient techniques are required. Walmsley et al. (2023b) trained deep learning models (Walmsley et al. 2023) on 10M Galaxy Zoo volunteer votes over 401k galaxies from the DESI Legacy Surveys to classify galaxy morphology based on this training data. Their models can typically predict what fraction of volunteers would give a particular answer to each question to within a mean vote fraction error of 10 per cent.

We match GZD within a 3" radius to the MPA-JHU SDSS DR7 catalogue (to obtain stellar masses, M_*, colours and emission line fluxes; Kauffmann et al. 2003; Salim et al. 2007) and the NYU-VAGC catalogue (to obtain k-corrections; Blanton et al. 2005), resulting in 793,824 galaxies. Figure 1 shows absolute r-band magnitude versus redshift for the entire sample (greyscale), as well as the disc galaxy sample (teal; described below).

2.2 Morphology Classification

In order to examine the secular growth, we select galaxies which are disc-dominated using GZD. The first classification the model must perform is to select whether the galaxy is "smooth and featureless", has "features or a disc", or contains (or is) an "artefact". To select disc-dominated galaxies, we require that the vote fraction for "features or disc" is $f_{\mathrm{smooth-or-featured\_featured-or-disk}} \geq 0.25$. This is visually
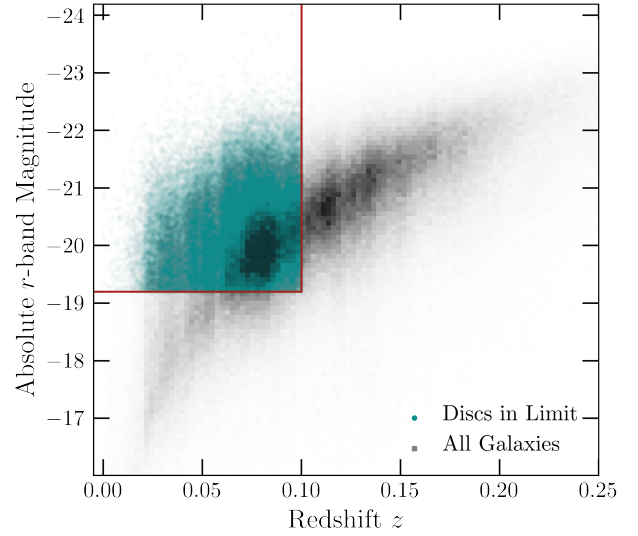
Figure 1. Absolute r-band magnitude against redshift, showing our volume limited sample. The grey-scale 2D histogram represents all galaxies in GZ DESI, and the teal points represent disc-dominated, not edge-on, merger-free galaxies within our volume limit. These teal points make up our full sample. The red lines at $M_r = -19.2$ and $z = 0.10$ delineate our redshift and r-band magnitude limits.

checked by the lead author (ILG). We also require that any discs must not be edge-on so that a bar can be identified if present, since in an edge-on galaxy, the bar can be obscured. GZD must categorise each featured galaxy as "edge on" or "not edge on", and for our purposes, we require $f_{\mathrm{disk-edge-on\_no}} \geq 0.5$. Galloway et al. (2015) examine the relationship between inclination angle and observed bar fraction, and they show (Figure 2) that the exact threshold used for "not edge on" does not have much of an effect. Our results also do not change significantly if $f_{\mathrm{disk-edge-on\_no}}$ is varied slightly.

To complete our sample, we require that the galaxy in the image does not appear to be merging with another galaxy. This is to ensure that our sample consists of galaxies grown via secular processes, and is not contaminated by AGNs which may be significantly fuelled by merger-driven mechanisms. GZD classifies every image with a merger class of "merger", "major disturbance", "minor disturbance", or "none". We consider galaxies with any significant level of disturbance to be potential contaminants to a sample of discs undergoing secular evolution. Thus we create a parameter we refer to as merger prominence, ζ_{avg}, analogous to the bulge prominence in Masters et al. (2019). We define ζ_{avg} as:

$$
\begin{aligned}
\zeta_{\mathrm{avg}} = {} & 0.2 \times f_{\mathrm{merging\_minor-disturbance}} \\
& + 0.8 \times f_{\mathrm{merging\_major-disturbance}} \\
& + f_{\mathrm{merging\_merger}}
\end{aligned}
\tag{1}
$$

We require our sample to contain only galaxies which are not merging, which we identify as $\zeta_{\mathrm{avg}} < 0.3$. This value has been visually checked to be consistent with undisturbed galaxies.

In addition to the above thresholds being in line with previous Galaxy Zoo studies, they have all been visually checked to ensure that they are reasonable and well aligned with the goals of this study.

In order to reduce selection effects, we select a volume-limited sample, having $z \leq 0.1$ and $M_r \leq -19.2$, as shown in Figure 1.
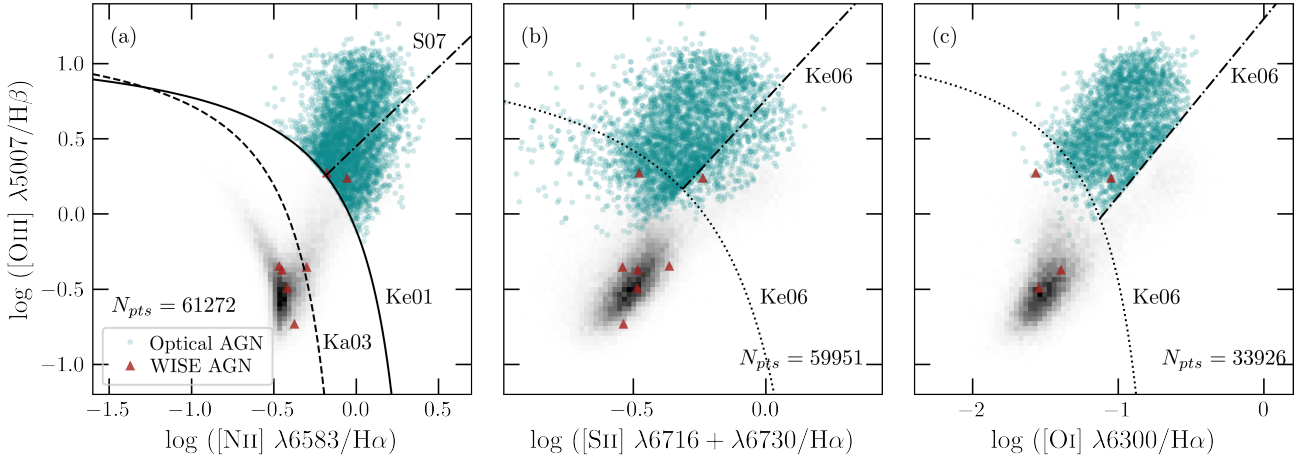
Figure 2. Classification of disc-dominated sources on a trio of BPT diagrams (Baldwin et al. 1981) From panel a, we assume that any source falling below the Ka03 line (Kauffmann et al. 2003) is purely star-forming. Anything above the Ke01 line (Kewley et al. 2001) is either an AGN or a LINER, and thus any source lying between those two lines is classed as composite. To distinguish between AGNs and LINERs, we use Panels (c), then (b), then a in that order. This is because where a source has S/N > 3 in [OI], then Panel (c) is the most reliable, and any source lying above the Ke06 (Kewley et al. 2006) line is an AGN, whereas below is a LINER. Where a source has S/N < 3 in [OI], but S/N > 3 in [SII], we use Panel (b). Again, a source lying above the Ke06 line is classified as an AGN and below is a LINER. Where both [SII] and [OI] in a source have S/N < 3, we use [NII]. Any source lying above the S07 line (Schawinski et al. 2007) is classified an AGN, and below is a LINER.

The 81,473 galaxies that form our final, complete sample (i.e., within the volume limit, disc dominated, face on, not merging) are shown in teal.

Within this volume-limited sample, we subsequently identify whether each of our galaxies has a bar, and the strength of that bar. GZD asks the models to distinguish between "strongly barred", "weakly barred", and "not barred". We classify a galaxy as unbarred if $f_{\text{no-bar}} > 0.5$. We then divide the barred galaxies into strong and weak bars in order to investigate the effect of bar strength on AGN presence. We say that a galaxy is strongly barred if $f_{\text{strong-bar}} \geq 0.35$ and $f_{\text{no-bar}} \leq 0.5$. Finally, we define a galaxy as being weakly barred is $f_{\text{strong-bar}} < 0.35$ and $f_{\text{no-bar}} \leq 0.5$. Again, these limits were determined via visual inspection by the lead author. This means that every galaxy in our disc sample is categorised as unbarred (NBAR, 27,480 galaxies), strongly barred (SBAR, 7877 galaxies) or weakly barred (WBAR, 46,116 galaxies).

2.3 Activity Classification

We use BPT diagrams (Baldwin, Phillips & Terlevich 1981) to classify the galaxies in our sample as either: undetermined, star-forming, composite, Type II AGN, or LINER. After performing k-corrections and extinction corrections, we use the emission lines from MPA-JHU DR7 to place galaxies on the diagram, and we show the distribution in Figure 2.

In order for a source to be classifiable according to this method, we require that the signal-to-noise ratio (S/N) in [OIII], Hβ, [NII] and Hα be S/N ≥ 3, in order to ensure good quality emission lines. If a galaxy does not fulfil this first requirement, it is classified as undetermined (20,199 galaxies). Using Panel (a) in Figure 2, we classify a galaxy as star-forming if it falls below the Ka03 line (Kauffmann et al. 2003, 37,218 galaxies). If a galaxy falls between the Ka03 line and the Ke01 line (Kewley et al. 2001), then it is classified as composite (13,735 galaxies), and the emission is likely due to a combination of star formation and AGN activity. If a galaxy falls above the Ke01

line, we classify it as either an AGN or a LINER (Low-Ionisation Nuclear Emission-line Region) as follows.

There are three different emission lines we can use to distinguish AGNs from LINERs - [SII], [OI] and [NII]. The most reliable line is [OI] (Kewley et al. 2006) and this should be used where possible, so if $S/N_{\text{[OI]}} \geq 3$, we can use Panel (c), and classify any source falling below the Ke06 line (Kewley et al. 2006) as a LINER (2,031 galaxies). This results in the hard cut-off line we see in Panel (c) that is not present in (a) or (b) for distinguishing between AGNs and LINERs. Where $S/N_{\text{[OI]}}$ is too low, [SII] is the next best emission line, and so if $S/N_{\text{[SII]}} \geq 3$ we can use Panel (b), and classify any source falling below the Ke06 line as a LINER (3,765 galaxies). Where both $S/N_{\text{[SII]}}$ and $S/N_{\text{[OI]}}$ are too low, we can resort to Panel (a), and use the S07 line (Schawinski et al. 2007), since a source must have $S/N_{\text{[NII]}} \geq 3$ in order to be classifiable at all. Anything both below this line and above the Ke01 line can be classified as an LINER (643 galaxies). This leaves us with 3,880 optically classified AGNs in our volume-limited disc sample.

Some AGNs are not optically classifiable, and are instead observable primarily in the infrared regime. We match our catalogue to the Wide-Field Infrared Survey Explorer (WISE) AGN catalogue (Assef et al. 2018), and any AGNs which are present in this catalogue, but not classified as AGNs according to the method described above, we add to our sample. There are 7 WISE AGNs which appear in our volume limited galaxy sample, 2 of which are classified as AGNs using BPT diagrams, so we can add reclassify an additional 5 galaxies as AGNs, to give us a total of 3,885 AGNs.

For a complete breakdown of how many galaxies are in each morphology category, and in each activity category, see Appendix A.
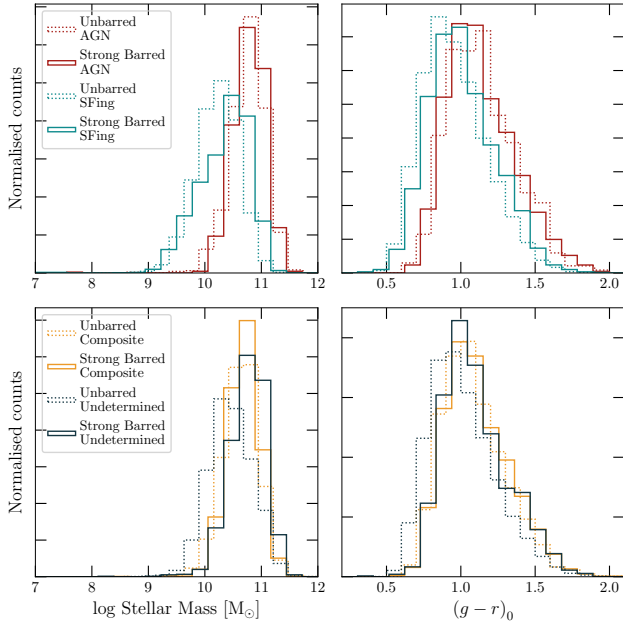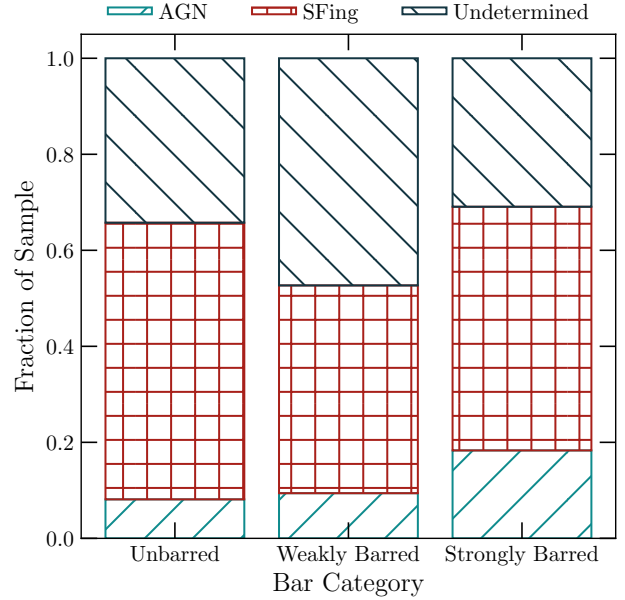
Figure 3. The distributions in M_* and $g - r$ colour for a variety of subsamples, with strongly barred galaxies in solid lines, unbarred in dashed lines, AGNs in red, star-forming in teal, composite in orange and undetermined in navy blue. Weakly barred galaxies are not shown for simplification, but lie between the strongly barred and unbarred samples.

Figure 4. The distribution of activity classification within each bar category, as shown in Table 1 AGN fraction is shown as positive diagonal in teal, star-forming (SFing) is shown as red square hatching, and Undetermined is shown as navy blue negative diagonal. Whilst in all three bar categories, the AGN fraction is the smallest contingent, the strongly barred galaxies have a noticeably greater fraction of AGN than the other categories. The weakly barred galaxies have a minor increase in AGN fraction compared to the unbarred galaxies.

3 RESULTS

We look at the variation in M_* and colour between strongly barred (SBAR), weakly barred (WBAR) and unbarred galaxies (NBAR), and the results are shown in Figure 3. For visualisation purposes, we omit the results for WBAR since they lie between the two other samples (however this inclusive plot in shown in Appendix B). As expected, the star-forming galaxies (teal) are less massive and slightly bluer than the AGN hosts (red). We can also see that the composite galaxies (orange) have overlap with both star-forming and AGN hosts, which confirms that their activity is due to a mixture of star formation and AGN. This is very similar to the undetermined galaxies (navy blue), whose signal to noise is too low to classify their activity. The undetermined galaxies are likely a mix of passively evolving and quenched disc galaxies. There are also some small differences between the barred and unbarred samples, with bars tending to reside in more massive, redder discs, particularly in both the star-forming samples and the undetermined samples, in agreement with previous studies (e.g., Masters et al. 2011).

For further analysis, we limit our sample to only star-forming, undetermined and AGN host galaxies to avoid any ambiguity from the LINER and composite samples.

We divide our sample of star-forming, undetermined and AGN host galaxies into our SBAR, WBAR and NBAR samples. Within these three samples, we divide the M_* and colour each into 15 bins of equal width, and assign weights to each galaxy, such that overall the M_* and colour distributions of SBAR, WBAR and NBAR are the same. This is because AGN presence is known to correlate with M_* and colour, and we want to reduce selection effects, and ensuring that the distributions are the same will aid this. We can then determine the fraction in each bar category of AGN, star-forming and undetermined

Table 1. The fraction of each activity category within each bar classification, as shown in Figure 4. AGN presence in strongly barred galaxies is around twice as prolific as in weakly barred or unbarred galaxies.

	Strongly Barred	Weakly Barred	Unbarred
AGN	18.3 ± 0.6	9.4 ± 0.4	8.1 ± 0.4
Star-forming	50.8 ± 0.8	43.3 ± 0.7	57.6 ± 0.7
Undetermined	30.9 ± 0.7	47.3 ± 0.6	34.3 ± 0.6

galaxies, and the weighted results are shown in Figure 4, and Table 1. Errors arise from the binomial distribution (Cameron 2011).

Given the small errors on each of these, it is highly unlikely that any of these subsamples are drawn from the same parent distribution. The difference between SBAR compared to both WBAR and NBAR is significantly greater than the more minor differences between WBAR and NBAR. These initial results indicate that AGNs are more likely to reside in strongly barred galaxies than either weakly barred or unbarred. However, given the ranges of M_* and colour, we endeavour to examine these fractions as a function of both, whilst simultaneously examining how these fractions may vary across M_*-colour space. Given the lack of similarity between star-forming and undetermined galaxies, we perform our comparisons with AGN host galaxies on each of these samples individually.

3.1 AGN hosts and star-forming galaxies

Including only AGN hosts and star-forming galaxies, we divide our sample into nine bins in M_* and nine bins in colour. Within each bin,

we calculate the AGN fraction in strongly barred galaxies, $f_{\mathrm{AGN,SBAR}}$ and the AGN fraction in unbarred galaxies, $f_{\mathrm{AGN,NBAR}}$. We then find the difference in these two fractions, and this is shown in Figure 5 on the first panel ('Strong v. Unbarred').

The difference between the two fractions is shown as a colour bar, where green indicates that the fraction of strongly barred galaxies which host AGNs is greater than the fraction of unbarred galaxies which host AGNs. In order to reduce noise, we only show bins where there are at least 10 AGNs in a bin. We can see that nearly every bin is green, with approximately $f_{\mathrm{AGN,SBAR}} - f_{\mathrm{AGN,NBAR}} \approx 0.2$. This is a small but significant increase in the number of AGNs in strongly barred galaxies.

When we repeat this analysis for WBAR and NBAR our result is qualitatively the same, but the signal is much less strong, indicating that any effect that weak bars have on AGN presence is less pronounced than for strong bars, which is also reflected in the lower fractions over the full M_*-colour-matched sample. This is plotted in the second panel of Figure 5. However, the AGN fraction is still higher in weakly barred galaxies than in disc galaxies without bars.

We can directly compare SBAR and WBAR across the M_*-colour diagram as well (Figure 5), and we find that the fraction of strongly barred galaxies hosting AGNs is significantly greater than the fraction of weakly barred galaxies hosting AGNs. However, this difference is not as strong as when we compare SBAR to NBAR.

Given that any increase in AGN fraction is so small, we check that this value is not overly dependent on binning, and we repeat these calculations for every M_* and colour bin combination from 5 bins to 17 bins.

For each binning combination, we calculate the median difference in AGN fraction (e.g. $f_{\mathrm{AGN,SBAR}} - f_{\mathrm{AGN,NBAR}}$), and we plot these medians in Panel (a) of Figure 6, with SBAR vs. NBAR in solid, dark blue, WBAR vs. NBAR in dashed teal, and SBAR vs. WBAR in dotted red.

If there was no difference in the likelihood of hosting an AGN between these three samples, we would expect the histograms to centre around 0 (e.g., $f_{\mathrm{AGN,SBAR}} - f_{\mathrm{AGN,NBAR}} = 0$) shown as a dash-dotted line. We always take the weaker bar category from the stronger bar category, so if the centre of the histograms is greater than 0, the stronger bar category is more likely to host an AGN than the weaker, and vice versa if the centre of the histogram is less than 0.

Looking at Figure 6, Panel (a), we can immediately see that in every case, the stronger bar category is more likely to host an AGN than the weaker bar category – strongly barred galaxies are more likely to host an AGN than weakly barred galaxies, which are in turn more likely to host an AGN than unbarred galaxies. Yet this excess of AGNs we see is very small.

A Shapiro-Wilk test (Shapiro & Wilk 1965) shows that we cannot reject Normality for the distribution of the medians for any case, with p-values in each case greater than $p_{\mathrm{SW}} > 0.15 \ (< 1.5\sigma)$ Thus, we can perform a simple T-test (Student 1908) to quantify the significance of this excess of AGN. In each of these cases, the p-value resulting from a T-test is $p_{\mathrm{T}} \ll 1 \times 10^{-6} \ (\gg 5\sigma)$, and thus we reject the hypothesis that the likelihood of each of these bar categories hosting an AGN is the same. Furthermore, we can say that in each case, the galaxies in the stronger bar category are more likely to host an AGN that the galaxies in the weaker bar category to a 5σ confidence.

For each binning combination, we also calculate the fraction of bins where the stronger bar category hosts a greater AGN fraction than the weaker bar category (e.g. $f_{\mathrm{AGN,SBAR}} > f_{\mathrm{AGN,NBAR}}$), and we plot these values in Panel (b) of Figure 6, with SBAR vs. NBAR in solid, dark blue, WBAR vs. NBAR in dashed teal, and SBAR vs. WBAR in dotted red.

For example, if we have 5x5 bins, and 20 bins have $f_{\mathrm{AGN,SBAR}} > f_{\mathrm{AGN,NBAR}}$, we would report a value of 0.8 for this bin combination. If there was no difference in the likelihood of hosting an AGN between our three samples, we would expect the distributions to centre around 0.5 – half of the bins would show a greater fraction of AGNs in one bar category than the other. This point is signified by a dash-dotted line.

Again, we perform a Shapiro-Wilk test for Normality. For the combinations WBAR vs. NBAR, and SBAR vs. WBAR, we obtain p-values of $p_{\mathrm{SW}} > 0.08 \ (< 1.7\sigma)$, and thus for these two samples, we can use a T-test to quantify the excess of bins containing a higher AGN fraction in the stronger bar category. In these two cases, the p-value resulting from a T-test is $p_{\mathrm{T}} \ll 1 \times 10^{-6} \ (\gg 5\sigma)$.

Since we cannot reject Normality for the case of SBAR vs. NBAR ($p_{\mathrm{SW}} = 0.00$), we must use the more conservative method of calculating the number of standard deviations the mean of the distribution is away from 0.5. With a mean value of 0.97, and a standard deviation, σ_{SD} of 0.03, we can say that the mean is $15\sigma_{\mathrm{SD}}$ away from 0.5, and therefore is not in agreement. Thus, in each case, the stronger bar category has an AGN fraction that is greater than the weaker bar category across the M_*-colour regime, meaning that there is not one specific combination of M_* and colour driving this relationship, further justifying that our results are not sensitive to the choice of binning.

3.2 AGN hosts and undetermined galaxies

We now seek to determine what effect a bar has on an AGN compared to a sample of undetermined disc galaxies (likely red spirals), in much the same way as in Section 3.1.

We plot the variation over M_*-colour space for each combination of bar category, and the results are shown in Figure 7. We can immediately see that there is a much more pronounced difference between SBAR and WBAR compared to the same plot involving star-forming galaxies. The increase in AGN fraction in SBAR compared to NBAR is not seen in WBAR compared to NBAR. Comparing SBAR to WBAR, we also have a very strong increase in AGN fraction with bar strength, indicating that strongly barred galaxies are significantly more likely to host an AGN than weakly barred.

Again, we want to confirm that our results are not dependent on binning, and so vary the number of bins in both M_* and colour from 5 to 17, and find the median value of the difference in AGN fraction and the fraction of bins where the stronger bar category has a higher AGN fraction than the weaker bar category. These statistics are shown in Figure 8.

First, examining Panel (a) in Figure 8, it can be seen that the relationships between SBAR vs. NBAR and SBAR vs. WBAR are both much stronger than WBAR vs. NBAR. In each case, SBAR galaxies are more likely to host an AGN than either other category. Comparing WBAR vs. NBAR, we actually see a histogram that appears consistent with 0. When we perform Shapiro-Wilk tests on these three histograms, we obtain p-values of $p_{\mathrm{SW}} > 0.065 \ (< 1.8\sigma)$, indicating that the histograms in Panel (a) are all consistent with Normality, and thus eligible for a T-test. The results of the T-test for SBAR vs. NBAR, and SBARvs. WBAR are $p_{\mathrm{T}} \ll 1 \times 10^{-6} \ (\gg 5\sigma)$. This is also the case for WBAR vs. NBAR, despite the fact that clearly the increase in AGN fraction is much smaller than in the other two comparisons.

Panel (b) in Figure 8, analogous to Panel (b) Figure 6 shows the fraction of bins where the AGN fraction in the stronger bar category is greater than the AGN fraction in the weaker bar category for each binning combination. Shapiro-Wilk tests on these three histograms
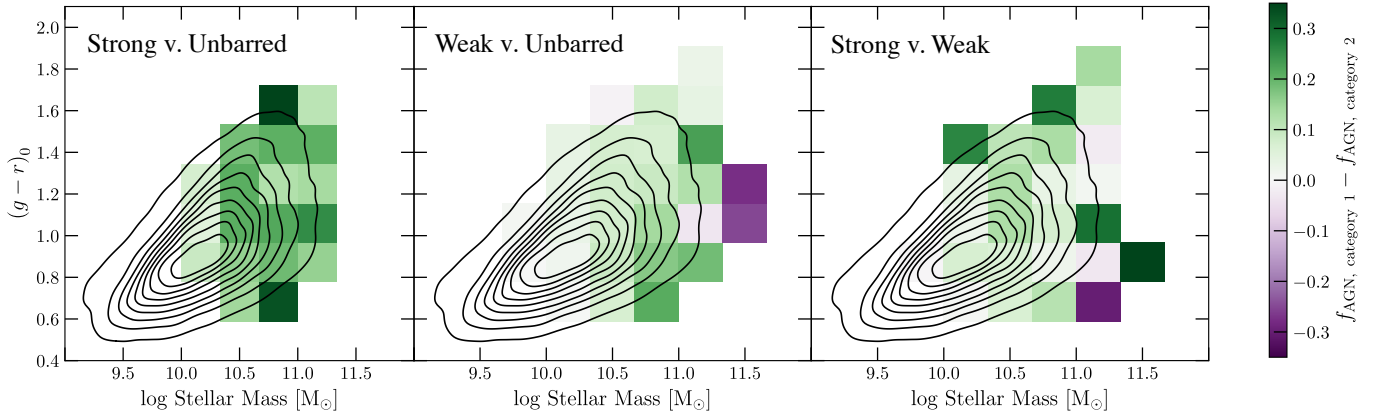
Figure 5. The difference between the AGN fraction in two bar categories for every combination of SBAR, WBAR and NBAR in a sample consisting of only AGN host galaxies and star-forming galaxies, with M_* on the x-axis and $g - r$ colour on the y-axis. In each case, the label in the upper left is written as 'Category 1 v. Category 2'. The black contours indicate the entire population of disc galaxies. The 2D histogram indicates the distribution of AGN-host disc galaxies, where there are a minimum of 10 AGN in a bin. Where the bin is more green, this indicates that the fraction of Category 1 galaxies hosting AGNs is greater than the fraction of Category 2 galaxies hosting AGNs. Where the bin is more purple, the reverse is true.
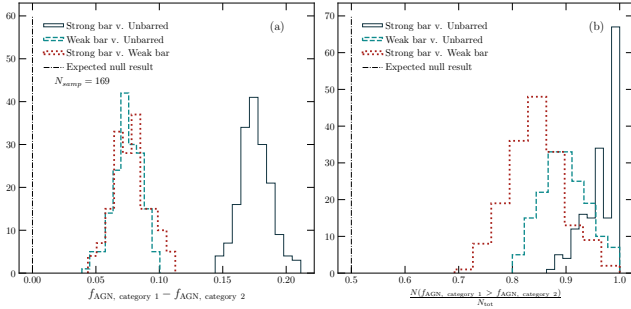
Figure 6. The distributions of the median difference between AGN fractions in Panel (a), and the distribution of the fraction of bins where Category 1 bars are greater than Category 2, in a sample consisting only of AGN-host galaxies and star-forming galaxies. In each case, the legend is written as 'Category 1 v. Category 2'. The black dashed-dotted lines indicate the expected mean of the distributions if bar presence did not affect AGN presence. The navy blue, solid lines represent SBAR v. NBAR. The teal, dashed lines represent WBAR v. NBAR. The red, dotted lines represent SBAR v. WBAR. The further to the left of the expected null result the histograms lie, the greater the tendency for AGN to lie in bar Category 1 galaxies.

all return p-values of $p_{SW} < 0.007$ ($> 2.6\sigma$), and thus we must reject Normality for all three comparisons.

We resort to using the more conservative method of determining the number of standard deviations away from 0.5 the mean of each distribution is. For SBAR vs. NBAR, the mean is 0.95, and the standard deviation is $\sigma_{SD} = 0.04$, making the mean $11\sigma_{SD}$ away from 0.5. For SBAR vs. WBAR the mean is 0.95, and the standard deviation is $\sigma_{SD} = 0.03$, making the mean $15\sigma_{SD}$ away from 0.5. Thus in these cases, we can reject the null hypothesis, and acknowledge that these comparisons are inconsistent with there being no difference between the two samples. For WBAR vs. NBAR, the mean is 0.54, and the standard deviation is $\sigma_{SD} = 0.05$, and thus we cannot reject the null hypothesis. WBAR and NBAR are consistent with being indistinguishable from each other across the M_*-colour diagram.

4 DISCUSSION

This result is statistically sound, and clarifies the debate over the last few years of how much of the observed effect of bars is simply down to selection effects. This is in agreement with studies such as Silva-Lima et al. (2022), who counter for selection effects and find that barred galaxies have a higher accretion parameter than unbarred, and that AGNs are found more commonly in galaxies with a bar. Since we are looking at incidence rather than luminosity or accretion, this study is particularly complementary. Given that Géron et al. (2023) showed that strong and weak bars must be considered separately, this could also be responsible for some of the discrepancies seen in previous studies (e.g. Cheung et al. 2013; Goulding et al. 2017; Zee et al. 2023), who find no correlation between bars and AGNs.

By splitting our comparison sample into 'star-forming' and 'undetermined', we can hone in on how the AGNs are correlated with bar presence in different environments. Crucially, undetermined galaxies are likely quiescent, red spirals, given their lack of emission lines (Masters et al. 2010; Galloway et al. 2015). Thus, they have significantly less cold gas than their star-forming counterparts, and this could be responsible for some of the differences we see.
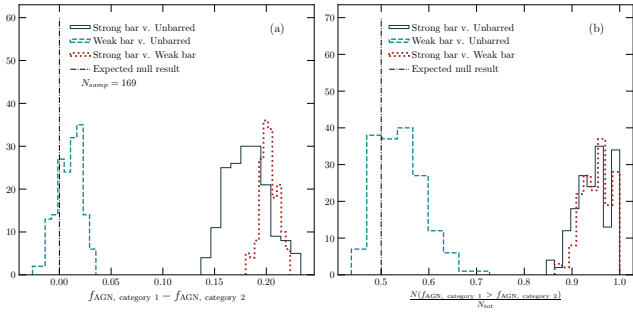
Both strong and weak bars can fuel AGNs, as seen in our comparison with star-forming galaxies. In the star-forming comparison sample, there was less likely to be a bar present. We postulate that were a bar present in a star-forming galaxy, strong or weak, this bar is efficient at fuelling gas down to the central kilo-parsec, where it can be accreted onto an AGN. This 'converts' the star-forming galaxy to an AGN host galaxy, after transitioning through the composite stage, according to the BPT diagrams (Figure 2). Thus we less commonly see star-forming galaxies with a bar.

In undetermined galaxies, weak bars are more commonplace than in AGN-host galaxies, since they are not efficient enough to funnel the poor gas reservoirs down to the central kiloparsec. This can more commonly be done by a strong bar, which converts the undetermined galaxy to an AGN host galaxy according to the BPT diagrams (Figure 2).

Work done by Géron et al. (2023) shows that strong and weak bars have different formation mechanisms; strong bars are triggered by global disc instabilities, whereas weak bars are formed through tidal interactions. Additionally, they show that strong bars have a slower

Figure 7. The difference between the AGN fraction in two bar categories for every combination of Sʙᴀʀ, Wʙᴀʀ and Nʙᴀʀ in a sample consisting of only AGN host galaxies and undetermined galaxies, with M_* on the x-axis and $g - r$ colour on the y-axis. In each case, the label in the upper left is written as 'Category 1 v. Category 2'. The contours indicate the entire population of disc galaxies. The 2D histogram indicates the distribution of AGN-host disc galaxies, where there are a minimum of 10 AGN in a bin. Where the bin is more green, this indicates that the fraction of Category 1 galaxies hosting AGNs is greater than the fraction of Category 2 galaxies hosting AGNs. Where the bin is more purple, the reverse is true.

Figure 8. The distributions of the median difference between AGN fractions in Panel (a), and the distribution of the fraction of bins where Category 1 bars are greater than Category 2, in a sample consisting only of AGN-host galaxies and undetermined galaxies. In each case, the legend is written as 'Category 1 v. Category 2'. The black dashed-dotted lines indicate the expected mean of the distributions if bar presence did not affect AGN presence. The navy blue, solid lines represent Sʙᴀʀ v. Nʙᴀʀ. The teal, dashed lines represent Wʙᴀʀ v. Nʙᴀʀ. The red, dotted lines represent Sʙᴀʀ v. Wʙᴀʀ. The further to the left of the expected null result the histograms lie, the greater the tendency for AGN to lie in bar Category 1 galaxies.

bar pattern speed than weak bars. Further work could be done to investigate the inflow rates that each of these bar types could sustain, and combining this with the gas availability could show why weak bars do not correlate with AGN presence compared to undetermined galaxies, as if they cannot provide as high an inflow rate as strong bars, they require more gas to trigger an AGN. It is also necessary to see whether the causes of these bars can fuel an AGN, and thus the AGN presence is not due to the bar directly, but rather due to the same mechanisms that caused the bar presence.

We do see some AGNs in unbarred galaxies, and higher resolution data may aid us in determining if there are smaller, nuclear bars present in these galaxies. If not, large-scale bars cannot be the only method of secularly growing black holes, even if they are a significant contributor.

Future work will investigate this phenomenon at more distant redshifts (Margalef-Bentabol et al., in prep.), and investigate how these

AGNs are fuelled as the bar fraction decreases out to higher redshifts. Facilities such as Euclid will provide us with greater sky coverage at better resolution than currently available, and so with an increase in data, we should be able to reduce noise in our samples.

5 CONCLUSIONS

Using information taken from the DESI catalogue, as well as Galaxy Zoo DESI morphologies and SDSS emission line strengths, we have explored the effect of large scale bars on the tendency for AGN signals in a volume limited sample of galaxies. We have ascertained that any differences seen are real, and not a result of binning or selection effects Our key findings can be summarised as follows:

• When comparing AGN-host galaxies to star-forming galaxies, and to undetermined galaxies, strongly barred galaxies are much more likely to host an AGN than weakly barred or unbarred galaxies

• When comparing AGN-host galaxies to star-forming galaxies, weakly barred galaxies are more likely to host an AGN than unbarred galaxies, but less so than strongly barred galaxies. However, when comparing AGN-host galaxies to undetermined galaxies, weakly barred galaxies are only very slightly more likely to host an AGN than their unbarred counterparts, and further work is needed on this specific relationship.

• These effects are seen across the M_*-colour diagram and are thus not driven by a specific combination of M_* and colour.

Future work needs to involve analysing how these fractions of AGNs in barred galaxies vary with redshift, and increase sample size with facilities such as Euclid and LSST to decrease any noise in our sample.

DATA AVAILABILITY

The data from GZD is available in Walmsley et al., accepted 2023. **will adapt this at submission depending on where Mike's paper is in the pipeline, either with citation or Mike's email**

Any other catalogues used are publicly available from the following locations:

- MPA-JHU:
https://wwwmpa.mpa-garching.mpg.de/SDSS/DR7/
- NYU-VAGC:
http://sdss.physics.nyu.edu/vagc/
- DESI Legacy Surveys:
https://www.legacysurvey.org/dr10/description/

Software

This research has made use of Topcat (Taylor 2005), an interactive graphical tool for analysis and manipulation of tabular data.

This research has made extensive use of the following Python packages:

- Astropy, a community-developed core Python package for Astronomy (Astropy Collaboration et al. 2013, 2018, 2022).
- Matplotlib, a 2D graphics package for Python (Hunter 2007).
- Numpy (Harris et al. 2020), a package for scientific computing.
- Scipy (Virtanen et al. 2020), a package for fundamental algorithms in scientific computing.

REFERENCES

Alonso S., Coldwell G., Duplancic F., Mesa V., Lambas D. G., 2018, A&A, 618, A149

Assef R. J., Stern D., Noirot G., Jun H. D., Cutri R. M., Eisenhardt P. R. M., 2018, ApJS, 234, 23

Astropy Collaboration et al., 2013, A&A, 558, A33

Astropy Collaboration et al., 2018, AJ, 156, 123

Astropy Collaboration et al., 2022, ApJ, 935, 167

Athanassoula E., 2003, MNRAS, 341, 1179

Baldwin J. A., Phillips M. M., Terlevich R., 1981, PASP, 93, 5

Blanton M. R., et al., 2005, AJ, 129, 2562

Cameron E., 2011, Publ. Astron. Soc. Australia, 28, 128

Cheung E., et al., 2013, ApJ, 779, 162

Coelho P., Gadotti D. A., 2011, ApJ, 743, L13

Friedli D., Benz W., 1993, A&A, 268, 65

Galloway M. A., et al., 2015, MNRAS, 448, 3442

Garland I. L., et al., 2023, MNRAS, 522, 211

Géron T., Smethurst R. J., Lintott C., Kruk S., Masters K. L., Simmons B., Stark D. V., 2021, MNRAS, 507, 4389

Géron T., et al., 2023, MNRAS, 521, 1775

Goulding A. D., et al., 2017, ApJ, 843, 135

Harris C. R., et al., 2020, Nature, 585, 357

Heckman T. M., Best P. N., 2014, ARA&A, 52, 589

Hinshaw G., et al., 2013, ApJS, 208, 19

Hunter J. D., 2007, Computing in Science and Engineering, 9, 90

Kauffmann G., et al., 2003, MNRAS, 346, 1055

Kewley L. J., Dopita M. A., Sutherland R. S., Heisler C. A., Trevena J., 2001, ApJ, 556, 121

Kewley L. J., Groves B., Kauffmann G., Heckman T., 2006, MNRAS, 372, 961

Knapen J. H., Shlosman I., Peletier R. F., 2000, ApJ, 529, 93

Kormendy J., Ho L. C., 2013, ARA&A, 51, 511

Laine S., Shlosman I., Knapen J. H., Peletier R. F., 2002, ApJ, 567, 97

Lin L.-H., Wang H.-H., Hsieh P.-Y., Taam R. E., Yang C.-C., Yen D. C. C., 2013, ApJ, 771, 8

Maciejewski W., Teuben P. J., Sparke L. S., Stone J. M., 2002, MNRAS, 329, 502

Martig M., Bournaud F., Croton D. J., Dekel A., Teyssier R., 2012, ApJ, 756, 26

Martin G., et al., 2018, MNRAS, 476, 2801

Masters K. L., et al., 2010, MNRAS, 405, 783

Masters K. L., et al., 2011, MNRAS, 411, 2026

Masters K. L., et al., 2019, MNRAS, 487, 1808

McAlpine S., Harrison C. M., Rosario D. J., Alexander D. M., Ellison S. L., Johansson P. H., Patton D. R., 2020, MNRAS, 494, 5713

Oh S., Oh K., Yi S. K., 2012, ApJS, 198, 4

Regan M. W., Teuben P. J., 2004, ApJ, 600, 595

Sakamoto K., 1996, ApJ, 471, 173

Salim S., et al., 2007, ApJS, 173, 267

Schawinski K., Thomas D., Sarzi M., Maraston C., Kaviraj S., Joo S.-J., Yi S. K., Silk J., 2007, MNRAS, 382, 1415

Shapiro S. S., Wilk M. B., 1965, Biometrika, 52, 591

Silva-Lima L. A., Martins L. P., Coelho P. R. T., Gadotti D. A., 2022, A&A, 661, A105

Smethurst R. J., et al., 2021, MNRAS, 507, 3985

Smethurst R. J., et al., 2023, MNRAS,

Student 1908, Biometrika, 6, 1

Taylor M. B., 2005, in Shopbell P., Britton M., Ebert R., eds, Astronomical
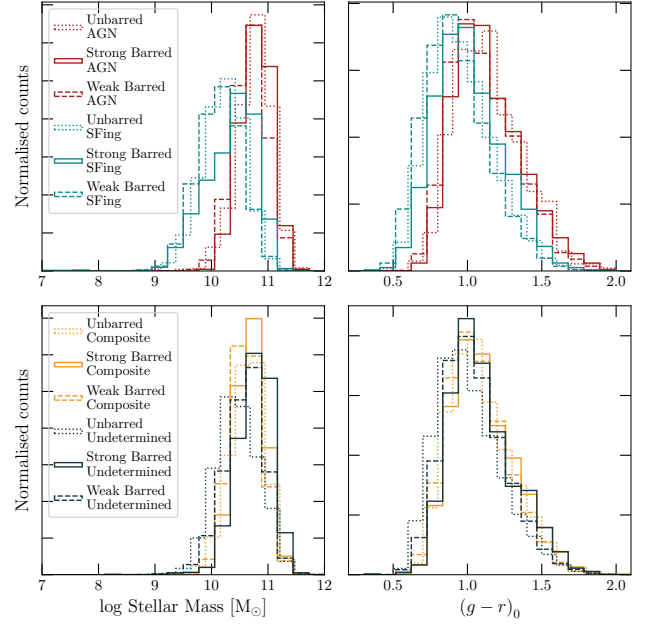
Figure B1. The distributions in stellar mass and $g - r$ colour for a variety of subsamples, with strongly barred galaxies in solid lines, unbarred in dotted lines and weakly barred in dashed lines. AGNs are in teal, star-forming in red, composite in orange and undetermined in navy blue.

Society of the Pacific Conference Series Vol. 347, Astronomical Data Analysis Software and Systems XIV. p. 29

Virtanen P., et al., 2020, Nature Methods, 17, 261

Walmsley M., et al., 2023, The Journal of Open Source Software, 8, 5312

York D. G., et al., 2000, AJ, 120, 1579

Zee W.-B. G., Paudel S., Moon J.-S., Yoon S.-J., 2023, ApJ, 949, 91

APPENDIX A: SUBSAMPLE COUNTS

APPENDIX B: FULL STELLAR MASS AND COLOUR DISTRIBUTIONS

This paper has been typeset from a TeX/LaTeX file prepared by the author.

Table A1. Full breakdown of the number of galaxies in each activity class, and each bar category, both in the volume limited sample, and before volume limiting.

Subsample Counts		
	Total	In Volume Limit
Is Disc	209402	81473
Is Undetermined	443659	82588
Is Star-forming	224276	72945
Is Composite	75872	30540
Is LINER	28826	15815
Is AGN	21183	7782
Is Disc and:		
Is Undetermined	72015	20199
Is Star-forming	88482	37218
Is Composite	30517	13735
LINER [O_I]	3014	2031
LINER [S_{II}]	5499	3765
LINER [N_{II}]	1058	643
Is LINER	9571	6439
Optical AGN	8804	3880
WISE AGN	26	7
Is AGN	8827	3885
Is Unbarred Disc and:		
Is Undetermined	20511	6292
Is Star-forming	30433	14933
Is Composite	7081	3650
LINER [O_I]	800	574
LINER [S_{II}]	1289	933
LINER [N_{II}]	247	157
Is LINER	2336	1664
Optical AGN	1819	941
WISE AGN	7	1
Is AGN	1826	942
Is Weak Barred Disc and:		
Is Undetermined	47492	12537
Is Star-forming	53397	20068
Is Composite	18857	7777
LINER [O_I]	1629	1017
LINER [S_{II}]	3316	2174
LINER [N_{II}]	686	404
Is LINER	5631	3595
Optical AGN	5456	2139
WISE AGN	18	6
Is AGN	5472	2143
Is Strong Barred Disc and:		
Is Undetermined	4012	1370
Is Star-forming	4652	2271
Is Composite	4579	2308
LINER [O_I]	585	440
LINER [S_{II}]	894	658
LINER [N_{II}]	125	82
Is LINER	1604	1180
Optical AGN	1529	800
WISE AGN	1	0
Is AGN	1529	800